Revealing the Presence of Potential Crossings in Diatomics Induced by Quantum Cavity Radiation

Johan F. Triana and José Luis Sanz-Vicario*
Grupo de Física Atómica y Molecular, Instituto de Física, Universidad de Antioquia, 050010-Medellín, Colombia

(Received 26 October 2018; revised manuscript received 15 December 2018; published 14 February 2019)

We propose an experiment to find evidence of the formation of light-induced crossings provoked by cavity quantum radiation on simple molecules by using state-of-the-art optical cavities, molecular beams, pump-probe laser schemes, and velocity mapping detectors for fragmentation. The procedure is based on prompt excitation and subsequent dissociation in a three-state scheme of a polar diatomic molecule, with two $^1\Sigma$ states (ground and first excited) coupled first by the UV pump laser and then by the cavity radiation, and a third fully dissociative state $^1\Pi$ coupled through the delayed UV/V probe laser. The observed enhancement of photodissociation yields in the $^1\Pi$ channel at given time delays between the pump and probe lasers unambiguously indicates the formation of a light-induced crossing between the two $^1\Sigma$ field-dressed potential energy curves of the molecule. Also, the production of cavity photons out of the vacuum field state via nonadiabatic effects represents a showcase of a molecular dynamical Casimir effect. To simulate the experiment outcome, we perform *ab initio* coherent quantum dynamics of the molecule LiF subject to external lasers and quantum cavity interactions in the strong coupling regime, using a product grid representation of the total polaritonic wave function for both vibrational and photon degrees of freedom.

DOI: 10.1103/PhysRevLett.122.063603

The interaction of molecules with intense ultrashort lasers has been an area of intense research in the last few decades, mostly without the need to introduce the quantum nature of radiation [1,2]. The more recent introduction of few-photon light sources along with optical cavities in quantum optics has opened a doorway to studying new phenomena emerging from the interaction of atoms and molecules with quantized radiation, and intriguing aspects in the photodynamics of molecules immersed in quantum optical cavities have brought new attention in the research community [3–6]. Nevertheless, most of the theoretical studies in this field are based on simplified model Hamiltonians which do not allow us to fully understand the detailed transformation of the molecular structure and dynamics under the effect of quantum radiation.

The introduction of quantum light implies that photons are denumerable, a situation which is described using a Fock basis $\{|n\rangle\}$. Alternatively, quantum radiation can be represented in coordinate space which avoids a large number of excitation manifolds with Fock polaritonic states [7,8]. In a recent study, we show that different quantum states of radiation may induce a different signature on the cavity molecular photodynamics [8]. One of the effects induced by radiation on matter systems is the formation of light-induced crossings (LIC) between the adiabatic potential energy curves (PEC) in systems with one nuclear degree of freedom or light-induced conical intersections (LICI) among adiabatic potential energy surfaces (PES) in systems with more than one nuclear coordinate [9,10]. Actually, the formation of LICI requires at least two dimensions for the energy degeneracy at the crossing. In diatoms, the extra coordinate is provided by the field polarization ϵ [10]. Radiation-matter interaction generates these LIC and LICI in both the semiclassical and quantum formulations of light. It must be noted that the fingerprints of the presence of LIC in diatomic molecules [11,12] have already been observed [13] under semiclassical conditions for light-matter interaction. However, the onset and inner workings of quantum light-induced LIC in molecules immersed in optical cavities have not been addressed so far.

Here we want to propose a *proof of principle* procedure to carry out an experiment producing a direct signature of the formation of a LIC in the simplest case of a diatomic polar molecule. The qualitative scheme of the experimental arrangement is pictured in Fig. 1. A high-Q optical cavity with two mirrors is located inside a vacuum chamber and arranged with the quantum radiation propagation axis in the laboratory $\hat{x}$ direction. A molecular beam of LiF prepared in a high-temperature oven is collimated with a skimmer along the $\hat{y}$ direction to enter the quantum cavity inside the vacuum chamber.

LiF molecules are randomly oriented while being transported within the molecular beam. Once LiF is inside the cavity, it is excited with an ultrashort UV pump laser pulse whose polarization axis lies along the $\hat{z}$ axis, and the

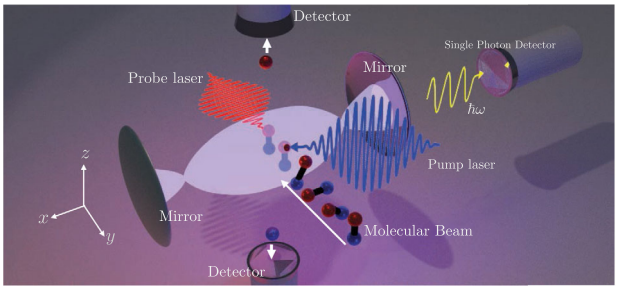

FIG. 1. Scheme for the experiment proposed to uncover cavity light-induced crossings with diatomic molecules.

propagation axis goes through the cavity in the plane $\hat{x}$-$\hat{y}$ (thus uncoupled with the cavity radiation). We are interested in the fragmentation of LiF along the $\hat{z}$ direction, and a Li (or F) fragment detector (up or down) is situated along the $\hat{z}$ direction. The UV laser produces dissociation for molecules oriented parallel (Σ–Σ transitions) and perpendicularly (Σ–Π transitions) to the laser polarization axis $\hat{z}$ because of known selection rules [14,15]. Consequently, those molecules oriented and then dissociated in the perpendicular orientation $\hat{x}$-$\hat{y}$ plane will not be detected by the $\hat{z}$ detectors. However, those LiF molecules inside the cavity already oriented parallel to the UV laser polarization make a prompt parallel transition from the ground electronic state $1^1\Sigma$ to the first excited $2^1\Sigma$ state (see Fig. 2).

In the absence of the quantum cavity, the expected nonadiabatic dynamics of LiF has been widely studied in the similar NaI case from the theoretical and experimental point of view by pioneering pump-probe techniques [16]. This scenario is equally valid for a LiF molecule, although with a faster dynamics. However, in the presence of a quantum cavity we have recently shown [8] that the LiF dynamics drastically changes because of the newly generated cavity LIC. The position of the LIC along the internuclear distance is determined by the crossing of the quantum dressed states, and its position R_{LIC} occurs at the internuclear distance where the cavity mode frequency ω_c is at resonance with the energy difference between the two coupled states, i.e., $\omega_c = E_{2^1\Sigma}(R) - E_{1^1\Sigma}(R)$ (atomic units are used unless otherwise stated). The interaction coupling for the LIC used in this work [17], $\chi\omega_c\sqrt{2}\hat{\mu}(R)\hat{x}$, depends not only upon the molecular dipole moment $\hat{\mu}_{1^1\Sigma-2^1\Sigma}(R)$, but also on the dipolar moment $\hat{x}$ associated with the quantum photon transitions. In fact, the transfer due to the LIC coupling can be stronger than that produced by the nonadiabatic crossing (NAC) located at $R = 13.1$ a.u. For a selected cavity mode frequency $\omega_c > 0$, an excited $2^1\Sigma$ wave packet (WP) starting at the Franck-Condon (FC) region reaches the position of the LIC prior to the NAC. In LiF, at the LIC position the WP splits into (i) a smaller portion that survives the LIC, remains in $2^1\Sigma$, and subsequently approaches the NAC (again with a second splitting and a portion leading to $1^1\Sigma$ dissociation), and (ii) a larger portion which transfers to

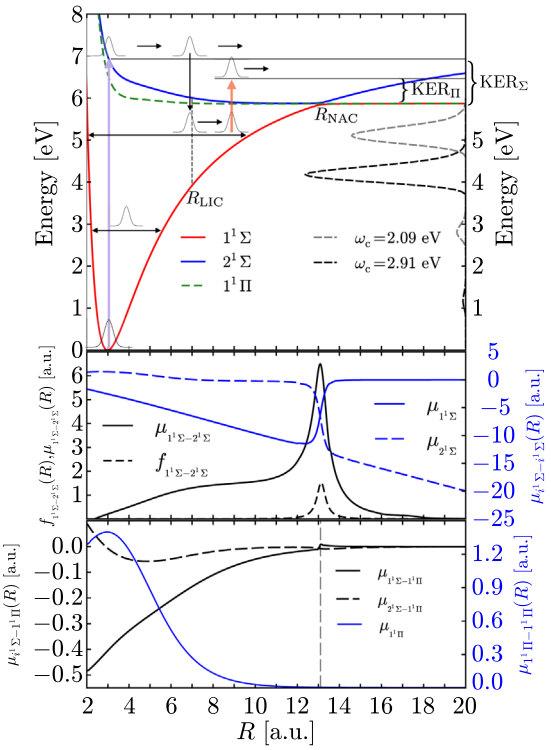

FIG. 2. *Top panel:* Potential energy curves of the lowest adiabatic $^1\Sigma$ and $^1\Pi$ states of LiF. The states corresponding to the $^1\Sigma$ symmetry display a (covalent-ionic) nonadiabatic avoided crossing at $R_{\mathrm{NAC}} = 13.1$ a.u. Pump-probe laser scheme: After a 7 eV UV laser pump, the molecular part of the polariton WP meets the LIC at $R_{\mathrm{LIC}} = 7$ a.u. for a cavity mode frequency $\omega_c = 2.09$ eV, and a delayed 1.5 eV probe laser pulse excites the polariton WP to the dissociating $^1\Pi$ state. Different kinetic energy releases (KER) can be distinguished as coming from the separate $^1\Sigma$ or $^1\Pi$ channels. The vibrational energy distributions of the $1^1\Sigma$ WP created by the cavity are also shown (see text), for cavity frequencies $\omega_c = 2.91$ eV (black solid line) and $\omega_c = 2.09$ eV (dashed grey line). *Middle panel:* Diagonal dipole moments $\mu_{1^1\Sigma}$ (blue solid line) and $\mu_{2^1\Sigma}$ (blue dashed line), and nondiagonal dipole moment $\mu_{1^1\Sigma-2^1\Sigma}$ (black solid line) for the two lowest states in LiF. The NAC between the two Σ states, $f_{1^1\Sigma-2^1\Sigma}$, is also included (black dashed line). *Bottom panel:* Diagonal dipole moment $\mu_{1^1\Pi}$ for the $^1\Pi$ state (blue solid line) and nondiagonal dipole moments $\mu_{1^1\Sigma-1^1\Pi}$ (black solid line) and $\mu_{2^1\Sigma-1^1\Pi}$ (black dashed line).

the $1^1\Sigma$ state, into a highly excited WP which bounces forth and back in the $1^1\Sigma$ state. This WP reflects from the outer turning point, and it eventually reaches again the position of the LIC, with a transfer back to the excited state $2^1\Sigma$. The last step implies a partial reconstruction of the initial WP, which then reproduces the whole process again [17]. This cavity induced cycle of recovering the initial state (in a few hundreds of femtoseconds) is much shorter than the cycle in absence of the cavity (a few picoseconds), and consequently, it also produces bursts of fragments through the NAC at a higher rate [8].

A notorious cavity effect is the production of bound excited states in the $1^1\Sigma$ state, some of them at low energy but mostly at high vibrational energies (Fig. 2), along with the side effect of production of cavity photons out of vacuum [8]. Such enhancement in the population of the intermediate highly excited states in $1^1\Sigma$ due to a LIC passage can then be monitored through the subsequent mapping of this bound WP by using a second delayed probe laser that pumps this population to measurable fragmentation resulting from a third fully dissociative state with Π symmetry [18], which is uncoupled to the Σ manifold by the cavity radiation.

Because of the form of the dipole $\mu_{1^1\Sigma-2^1\Sigma}(R)$ and the location of the LIC (far away from the FC region), the cavity is hardly able to excite LiF molecules already immersed in the cavity from the ground state in $1^1\Sigma$. The cavity coupling is much more evident for a dynamics starting from the $2^1\Sigma$ state. Thus, the UV pump laser initiates the nonadiabatic dynamics by copying the ground state to the $2^1\Sigma$ state, which then evolves toward the LIC and NAC internuclear positions. In our multiconfigurational time-dependent Hartree (MCTDH) [19] 2D simulations [17], we prepare a polariton state with the excited WP located at the FC region in the $2^1\Sigma$ state times the vacuum photon state $|0\rangle$ (represented in coordinate space). The total time-dependent polariton ket state for the three electronic states involved (ground plus two excited) can be written in the form $\langle R, x|\Psi(t)\rangle = \varphi_{1\Sigma}(R,x,t)|1\Sigma\rangle + \varphi_{2\Sigma}(R,x,t)|2\Sigma\rangle + \varphi_{1\Pi}(R,x,t)|1\Pi\rangle$ [8], where $\varphi_i(R,x,t)$ represents the (photon-matter) entangled WP for the vibrational R and cavity photon x coordinates moving within the electronic state i. The polariton WP splits for the propagation in the 2D adiabatic PES $V_i(R,x) = E_i(R) + \frac{1}{2}\omega_c^2 x^2 + \chi\omega_c\sqrt{2\hbar}\mu_i(R)x$, for $i = (1^1\Sigma, 2^1\Sigma, 1^1\Pi)$. Note that we neither include explicitly a LIC in the Hamiltonian nor use a light-dressed basis set of molecular states for our calculations; it develops by itself due to the cavity interaction using undressed bases.

The cavity photodynamics of LiF is dominated by two key effects: the action of LIC and NAC, where nonadiabatic transitions of different nature are effective, and consequently, the light-matter WP evolves as an entangled nonseparable state. For instance, for two chosen cavity mode frequencies $\omega_c = 2.91$ eV and $\omega_c = 2.09$ eV, Fig. 3 shows the time evolution of the global polariton populations for both the $1^1\Sigma$ and $2^1\Sigma$ states. In the time window 30–60 fs, the WP reaches the LIC region, where a strong population exchange occurs (the WP reaches $R_{\mathrm{LIC}} = 6$ a.u. for $\omega_c = 2.91$ eV earlier than it reaches $R_{\mathrm{LIC}} = 7$ a.u. for $\omega_c = 2.09$ eV). The second transfer of population happens at 80–110 fs due to the passage across the NAC at $R_{\mathrm{NAC}} = 13.1$ a.u. The next population exchange occurs at 140–150 fs for $\omega_c = 2.91$ eV and at ~200–220 fs for $\omega_c = 2.09$ eV, which corresponds to the slow passage across the LIC of the highly excited bound WP in $1^1\Sigma$ to the

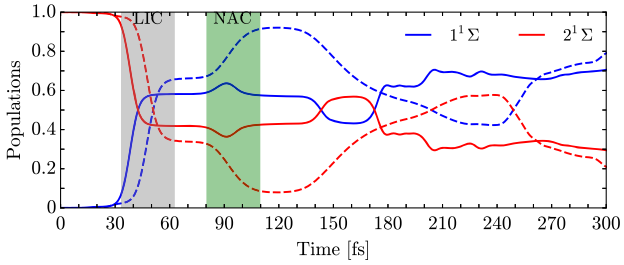

FIG. 3. Time-dependent polaritonic populations corresponding to the adiabatic states $1^1\Sigma$ and $2^1\Sigma$ for LiF, initially fully excited in the latter state and coupled with the radiation present in a cavity in the form of the Fock vacuum state $|0\rangle$, with interaction strength $\chi = 0.01$. Probabilities are included for two different cavity mode frequencies, $\omega_c = 2.91$ eV (solid lines) and $\omega_c = 2.09$ eV (dashed lines). Shaded regions correspond to the time windows for the first passage across the LIC region (gray) and the NAC region (green).

$2^1\Sigma$ state, during the contraction of the LiF bond after the reflection at the outer turning point of the $1^1\Sigma$ potential energy curve. This ultimately implies a partial reconstruction of the initial $2^1\Sigma$ WP. The same cycle starts again with this residual $2^1\Sigma$ polaritonic WP moving outward to the next LIC transfer at 170–180 fs for $\omega_c = 2.91$ eV and at 250–260 fs for $\omega_c = 2.09$ eV. The noticeable difference in population exchange at the time window 80–110 fs for $\omega_c = 2.91$ and 2.09 eV is because in the former case, although the $1^1\Sigma$ population increases due to the NAC transfer to dissociation, simultaneously the $1^1\Sigma$ bound WP transfers back to the $2^1\Sigma$ state through the LIC (producing a small hump). In the latter case, the actions of the NAC and the LIC are instead quite separated in time. In this respect, note that although for $\omega_c = 2.09$ a.u. the LIC is located at $R_{\mathrm{LIC}} = 7$ a.u., the bound WP has a higher excitation than for $\omega_c = 2.91$ a.u., thus with a longer excursion toward the outer turning point and backward to the LIC (see Fig. 2). In this case, it means that the $2^1\Sigma$ WP reaches the NAC before the $1^1\Sigma$ bound WP arrives again at the LIC.

The dynamics shown in Fig. 3 indicates time windows at which the LIC is more active. In this way a probe laser with a controlled time delay with respect to the UV laser may be able to monitor the abrupt change of population of the excited WP in $1^1\Sigma$, which is the witness for the passage through a LIC. In our MCTDH simulation, we are using a probe laser pulse $E(t) = E_0 f(T, t-\tau)\sin[\omega(t-\tau)]$ with a sine square envelope function $f(t)$, duration $T = 35$ fs, and with a tunable delay τ between $t = 0$ (pump laser excitation) and the center of the probe pulse, a central frequency ω from 1.5 to 2.5 eV, and an intensity slightly above 10^{14} W/cm^2 [17]. This second probe laser is focused into the cavity in the reaction volume (molecular and laser beams) with a polarization set in the $\hat{x} - \hat{y}$ plane, and is thus perpendicular to the pump laser polarization along $\hat{z}$. For the small time delays necessary to uncover LIC effects in

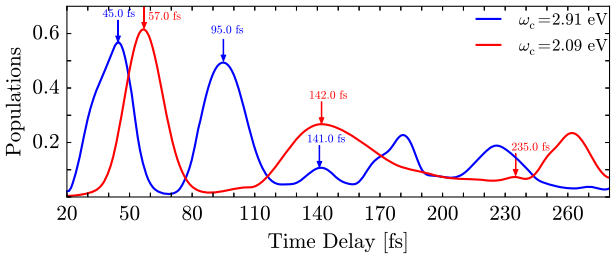

FIG. 4. Final population of the $^1\Pi$ excited state as a function of the pump-probe time delay τ for two cavity mode frequencies ω_c using different probe laser frequencies. Numerical values of delays for the first three maxima in the dissociation yields are indicated.

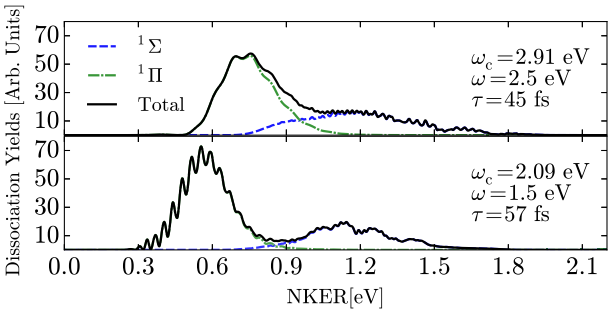

FIG. 5. Dissociation yields of the adiabatic electronic states $1^1\Sigma$ and $^1\Pi$ in terms of the nuclear kinetic energy release (NKER) for different cavity mode frequencies ω_c and different central frequencies ω of the probe pulse. The NKER spectra is calculated for the time delay corresponding to the first maximum included in Fig. 3.

our LiF showcase, the essential dynamics happens in the femtosecond time domain (vibration and dissociation), much faster than molecular rotation in the picosecond time window. Consequently, the LiF molecule barely rotates during the pump-probe time delay (molecular rotation is neglected in our calculations), and the axial recoil approximation [24] applies, so that the fragments arriving at the detectors on the $\hat{z}$ axis come from molecules already oriented in the same $\hat{z}$ direction at the time of pump excitation. Furthermore, both the $\hat{z}$-polarized pump laser (parallel Σ–Σ transitions) and the ($\hat{x}$-$\hat{y}$)-polarized probe pulse (perpendicular Σ–Π transitions) generate fragmentation along the same $\hat{z}$ axis.

Figure 4 shows the population of the third $1^1\Pi$ state against the pump-probe time delay for both cavity mode frequencies, $\omega_c = 2.91$ eV and $\omega_c = 2.09$ eV. Since the central energies of the vibrational distribution of the bound $1^1\Sigma$ WP for these two mode frequencies are separated by $\sim$1 eV, we choose a probe central frequency of $\omega_{\text{probe}} = 2.5$ eV for $\omega_c = 2.91$ eV and $\omega_{\text{probe}} = 1.5$ eV for $\omega_c = 2.09$ eV to reach a similar energy region in the $^1\Pi$ state. In the case of $\omega_c = 2.91$ eV, we find three maxima in the $^1\Pi$ population in the range $\tau \in [1, 160]$ fs. The first peak at $\tau = 45$ fs corresponds to the first passage of the excited $2^1\Sigma$ WP across the LIC (Fig. 3) with the corresponding efficient transfer $2^1\Sigma \to 1^1\Sigma$, which is promptly monitored by the probe laser by the transfer $1^1\Sigma \to 1^1\Pi$ [17]. The lowest $^1\Pi$ state is fully dissociative, with channel $\text{LiF}(1^1\Pi) \to \text{Li}(^2S) + \text{F}(^2P_{1/2})$, and it has an asymptotic energy which is only 0.003 a.u. above the lowest covalent Σ dissociation $\text{LiF}(1^1\Sigma) \to \text{Li}(^2S) + \text{F}(^2P_{3/2})$ due to spin-orbit coupling in F. However, fragments produced by both channels can be distinguished, because the nuclear kinetic energy release (NKER) of the Σ channel is unambiguously determined by the FC absorption, whereas the NKER of the Π channel does not follow a simple FC rule because of the flat shape of the $1^1\Pi$ potential energy curve at the LIC position, and it depends on the frequency ω_{probe} applied (Fig. 2). The second major peak appears at $\tau \sim 95$ fs, due to a second passage through the LIC, this time by the inward motion of the bound $1^1\Sigma$ WP. The third (much reduced) maximum signal for $^1\Pi$ dissociation in Fig. 4 at 141 fs for $\omega_c = 2.91$ eV comes again from a LIC passage. This time, it comes from the residual part of the $1^1\Sigma$ bound WP that moves outward from the inner turning point to $R_{\text{LIC}} = 6$ a.u..

The $2^1\Sigma$ WP is partially reconstructed in the interval $t \in [140, 170]$ fs, and the whole dynamical cycle repeats again with another three analogous consecutive peaks at $\tau = 180$, 225, and 270 fs with smaller intensities. Then, the selected peaks in the $^1\Pi$ population are associated with LIC passages, and they must produce enhancement in the fragment detection in the $\hat{z}$ direction. The analysis for $\omega_c = 2.09$ eV in Fig. 4 follows identically, although larger time delays are required to retrieve a similar physics. Here the first three peaks are located at 57, 142, and 235 fs, and the peak shown at 262 fs corresponds indeed to the first peak of the next cycle.

Finally, we show in Fig. 5 that fragments coming from the $1^1\Pi$ channel can be distinguished and separated kinematically from those corresponding to the $1^1\Sigma$ channel. Both dissociations yield neutrals, and the small energy separation between the two different spin-orbit coupled states of F does not allow for an easy spectroscopic discrimination. However, we show that the nuclear kinetic energy release (NKER) distribution for fragmentation in the $^1\Sigma$ channel is always centered at 1.2 eV (determined by the FC excitation), whereas the NKER distribution of fragments in the $^1\Pi$ channel is movable by the chosen probe frequency ω, and its signal can be well separated. In this sense, our symbolic detectors may indicate, for instance, the use of electron-impact ionization on Li fragments prior to entering a (quadrupolar) mass spectrometer to separate fast $(1^1\Sigma)$ and slow $(1^1\Pi)$ Li^+ ions.

Incidentally, we also find that transitions due to cavity LICs from initially excited molecular states involve the generation of photons inside the cavity out of vacuum. In our showcase we start from vacuum state $|0\rangle$, and we end up with photon state $|1\rangle$ after each LIC passage, or even

more photons due to the non-negligible diagonal dipole moment $\mu_{1^1\Sigma}$ and $\mu_{1^1\Pi}$ [8]. These cavity photons are just generated due to nonadiabatic mechanisms, which are conceptually related to the dynamical Casimir effect [25]. Single photon detectors situated along the $\hat{x}$ axis may eventually detect in coincidence these Casimir photons escaping through the cavity mirrors. To conclude, we have shown that intricacies of new polaritonic molecular dynamics involving nonadiabatic effects induced by quantum radiation can be linked to measurable quantities in the laboratory.

We thank Luis Bañares and Leonardo Pachón for useful discussions. This work was financially supported by Universidad de Antioquia (Vicerrectoría de Investigación) under Estrategia de Sostenibilidad and from Departamento Administrativo de Ciencia, Tecnología e Innovación (Colciencias, Colombia), under Grant No. 111565842968.

*Corresponding author.
jose.sanz@udea.edu.co

[1] F. Grossmann, *Theoretical Femtosecond Physics: Atoms and Molecules in Strong Laser Fields*, 3rd ed. (Springer Verlag, Berlin, 2018).
[2] A. Palacios, J. L. Sanz-Vicario, and F. Martín, J. Phys. B **48**, 242001 (2015).
[3] J. Galego, F. J. Garcia-Vidal, and J. Feist, Phys. Rev. X **5**, 041022 (2015).
[4] F. Herrera and F. C. Spano, Phys. Rev. Lett. **116**, 238301 (2016).
[5] J. Flick, M. Ruggenthaler, H. Appel, and A. Rubio, Proc. Natl. Acad. Sci. U.S.A. **114**, 3026 (2017).
[6] R. F. Ribeiro, L. A. Martínez-Martínez, M. Du, J. Campos-González-Angulo, and J. Yuen-Zhou, Chem. Sci. **9**, 6325 (2018).
[7] M. Kowalewski, K. Bennett, and S. Mukamel, J. Phys. Chem. Lett. **7**, 2050 (2016).
[8] J. F. Triana, D. Peláez, and J. L. Sanz-Vicario, J. Phys. Chem. A **122**, 2266 (2018).
[9] N. Moiseyev, M. Šindelka, and L. S. Cederbaum, J. Phys. B **41**, 221001 (2008).
[10] C.-C. Shu, K.-J. Yuan, D. Dong, I. R. Petersen, and A. D. Bandrauk, J. Phys. Chem. Lett. **8**, 1 (2017).
[11] G. J. Halász, M. Šindelka, N. Moiseyev, L. S. Cederbaum, and A. Vibók, J. Phys. Chem. A **116**, 2636 (2012).
[12] T. Szidarovszky, G. J. Halász, A. G. Császár, L. S. Cederbaum, and A. Vibók, J. Phys. Chem. Lett. **9**, 2739 (2018).
[13] A. Natan, M. R. Ware, V. S. Prabhudesai, U. Lev, B. D. Bruner, O. Heber, and P. H. Bucksbaum, Phys. Rev. Lett. **116**, 143004 (2016).
[14] G. Herzberg, *Molecular Spectra and Molecular Structure: Spectra of Diatomic Molecules* (Van Nostrand, New York, 1950).
[15] H. Lefebvre-Brion and R. W. Field, *Perturbations in the Spectra of Diatomic Molecules* (Academic Press, New York, 1986).
[16] A. Mokhtari, P. Cong, J. L. Herek, and A. H. Zewail, Nature (London) **348**, 225 (1990).
[17] See Supplementary Material at http://link.aps.org/supplemental/10.1103/PhysRevLett.122.063603 for details on the dipole formulation and computations, which includes Refs. [5,8,18–23].
[18] A. Tóth, P. Badankó, G. J. Halász, A. Vibók, and A. Csehi, Chem. Phys. **515**, 418 (2018).
[19] G. Worth, M. Beck, A. Jäckle, and H. Meyer, *The MCTDH Package, Version 8.4* (2007), http://mctdh.uni-hd.de.
[20] H.-J. Werner *et al.*, *Molpro, Version 2015.1, A Package of ab initio Programs* (2015), http://www.molpro.net.
[21] V. Rokaj, D. M. Welakuh, M. Ruggenthaler, and A. Rubio, J. Phys. B **51**, 034005 (2018).
[22] J. Fregoni, G. Granucci, E. Coccia, M. Persico, and S. Corni, Nat. Commun. **9**, 4688 (2018).
[23] H. Meyer, F. Gatti, and G. Worth, *Multidimensional Quantum Dynamics: MCTDH Theory and Applications* (John Wiley & Sons, New York, 2009).
[24] R. N. Zare, J. Chem. Phys. **47**, 204 (1967).
[25] V. V. Dodonov, Phys. Scr. **82**, 038105 (2010).

Supplementary Material: Revealing the presence of potential crossings in diatomics induced by quantum cavity radiation.

Johan F. Triana and José Luis Sanz-Vicario

Grupo de Física Atómica y Molecular, Instituto de Física, Universidad de Antioquia, Medellín, Colombia.

Here we provide the technical details about the electronic structure of LiF and the corresponding nuclear dynamics of the molecule coupled to a cavity mode as implemented in the multiconfigurational time-dependent Hartree (MCTDH) method. We also discuss some details on the inner workings of the non-adiabatic polariton photodynamics of LiF in the cavity.

A. Lithium Fluoride potential energy curves

The potential energy curves (PEC) of the two lowest $^1\Sigma$ and the lowest $^1\Pi$ electronic states of LiF and its corresponding couplings (dipolar and nonadiabatic) are calculated at the multi-reference configuration interaction (MRCI) level of theory, using the molecular electronic structure package MOLPRO [1]. Calculations for both PEC and couplings have been performed with a complete active space (CAS) using a multiconfigurational self-consistent field (MCSCF) method, then followed by a MRCI method, using the aug-cc-pVQZ basis set, 12 active electrons and 6 active orbitals. In particular, the non-adiabatic couplings between the two $^1\Sigma$ states have been calculated using a finite differences method for the derivatives and using the MRCI electronic wave functions. These lowest states compare identically with those in a recent calculation [2].

B. Hamitonian, dipole formulation and dynamic equations

The total time-dependent polariton ket state for the three electronic states involved (ground plus two excited) can be written in the form $\langle R, x|\Psi(t)\rangle = \varphi_{1^1\Sigma}(R,x,t)|g\rangle + \varphi_{2^1\Sigma}(R,x,t)|e_1\rangle + \varphi_{1^1\Pi}(R,x,t)|e_2\rangle$ [3], where $\varphi_i(R,x,t)$ represents the (photon-matter) entangled wave packet for the vibrational R and cavity photon x coordinates. This coordinate representation of radiation with mode frequency ω_c avoids the representation in terms of a large Fock space for photons and it indicates that the p-polarized quantum electric field within a cavity of volumen V, $\hat{E}_p = E_0(\hat{a} + \hat{a}^\dagger)\hat{\mathbf{e}}_p$, with $E_0 = \sqrt{\frac{\hbar\omega_c}{V\varepsilon_0}}$, can be also written in coordinate space, since $(\hat{a} + \hat{a}^\dagger) = \sqrt{\frac{2\omega_c}{\hbar}}\hat{x}$.

The full Hamiltonian for our system has the form:

$$\hat{H} = \hat{H}_{\text{Mol}} + \hat{H}_{\text{Cav}} + \hat{H}_{\text{Laser}} \tag{1}$$

where $\hat{H}_{\rm Mol}$ corresponds to the nuclear Hamiltonian of LiF, the Hamiltonian for the quantum cavity is [4]

$$\hat{H}_{\rm Cav} = \frac{1}{2}\hat{p}^2 + \frac{1}{2}\omega_{\rm c}^2\left(\hat{x} + \frac{\lambda}{\omega_{\rm c}}\hat{\mu}(R)\right)^2, \tag{2}$$

where λ is the dipole coupling strength (here we use instead $\chi = \frac{\lambda}{\sqrt{2\hbar}} = \frac{1}{\sqrt{\hbar V \varepsilon_0}}$) and $\hat{\mu}(R)$ is the molecular dipole moment, and the interaction with the external laser field $\mathbf{E}(t)$ is assumed in the semiclassical form $\hat{H}_{\rm Laser} = -\hat{\mu}(R)\mathbf{E}(t)$. Consequently the cavity Hamitonian contains the harmonic oscillator Hamiltonian plus the radiation-matter interaction in the cavity with the form $\chi\omega_{\rm c}\sqrt{2\hbar}\hat{\mu}(R)\hat{x} + \chi^2[\hat{\mu}(R)]^2$, with two dipole moment operators acting simultaneously in the first term, one for the molecule and another for the cavity photons. The second term, named quadratic dipole self-energy, does not depend on the photon displacement coordinate. The particular importance to include the self-energy term (gauge invariance, energy spectrum bounded from below, etc.) has been recently discussed elsewhere [4, 5] and it brings interpretations on the photon coordinate. LiF has a ionic dissociating channel along the $2^1\Sigma$ adiabatic state with a permanent dipole $\hat{\mu}_{2^1\Sigma}(R)$ (see Figure 2 in main text) which increases linearly with the internuclear distance R. To ensure that polaritonic energies within the $2^1\Sigma$ are bound from below, the dipole self-energy term is required. However, in our particular case, this self-energy term can be removed without consequences in the present results, for several reasons: i) our fragmentation observables come out from channels $1^1\Sigma$ and $1^1\Pi$, whose permanent dipoles $\mu_{1^1\Sigma}$ and $\mu_{1^1\Pi}$ vanish for large R (see Figure 2 in main text) , ii) The number of photons involved is our showcase are small (vacuum $|0\rangle$, one $|1\rangle$ and two $|2\rangle$ photon states), which are packed close to $x = 0$ in the photon coordinate, a region where the diagonal dipole term $\chi\omega_{\rm c}\sqrt{2\hbar}\hat{\mu}(R)\hat{x}$ barely corrects the $2^1\Sigma$ molecular potential energy curve, iii) the coupling constant used in this work is $\chi = 0.01$, for which the ground state potential energy curve still supports a long-living metastable state, iv) the displayed effects on fragmentation are the result of a fast dynamic process within the fs time window. In fact, we have tested our results against the inclusion or absence of the dipole self-energy term and we cannot find notorious differences in the dissociation yield of $^1\Pi$ channel (see figure 1). Thus, for the sake of simplicity, we only keep the terms already present in the familiar Jaynes-Cummings Hamiltonian (without rotating wave approximation). Similar conclusions in recent molecule-cavity non-adiabatic calculations can be found in [6].

With the three-state ansatz for the total wave packet we study the dynamics by solving the

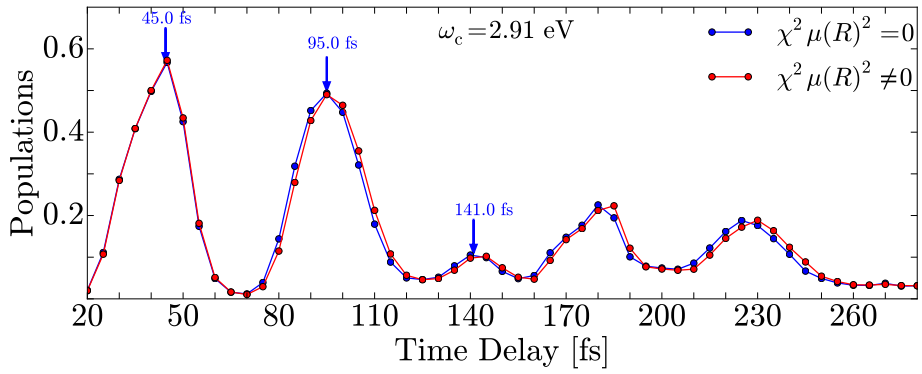

FIG. 1. Final population of the $^1\Pi$ excited state as a function of the pump-probe time delay τ for cavity mode frequency $\omega_c = 2.91$ eV, with and without the quadratic dipole self-energy term $\chi^2[\mu(R)]^2$ in the dynamical equations. Numerical values of delays for the first three maxima in the dissociation yields are indicated.

time dependent Schrödinger equation (TDSE), $\left(i\hbar\frac{d}{dt} - \hat{H}\right)|\Psi(t)\rangle = 0$. The full Hamiltonian, represented in our three-state electronic basis $(1^1\Sigma, 2^1\Sigma, 1^1\Pi)$, with the (simplified) cavity radiation interaction plus external classical laser pulses $\mathbf{E}(t)$, can be expressed in the form:

$$\hat{H}_{\rm Mol} = -\frac{\hbar^2}{2\mu}\frac{\partial^2}{\partial R^2}\cdot\mathbf{1} + \begin{pmatrix} E_{1^1\Sigma}(R) & \Lambda_{1^1\Sigma-2^1\Sigma}(R) & 0 \\ \Lambda_{1^1\Sigma-2^1\Sigma}(R) & E_{2^1\Sigma}(R) & 0 \\ 0 & 0 & E_{1^1\Pi}(R) \end{pmatrix} \tag{3}$$

$$\hat{H}_{\rm Field} = \left(-\frac{1}{2}\frac{\partial^2}{\partial x^2} + \frac{1}{2}\omega_c^2 x^2\right)\cdot\mathbf{1} \tag{4}$$

$$\hat{H}^{\rm I}_{\rm Mol-Field} = \begin{pmatrix} \chi\omega_c\sqrt{2\hbar}\mu_{1^1\Sigma}(R)x & \chi\omega_c\sqrt{2\hbar}\mu_{1^1\Sigma-2^1\Sigma}(R)x & \mu_{1^1\Sigma-1^1\Pi}(R)\cdot\boldsymbol{E}(t) \\ \chi\omega_c\sqrt{2\hbar}\mu_{1^1\Sigma-2^1\Sigma}(R)x & \chi\omega_c\sqrt{2\hbar}\mu_{2^1\Sigma}(R)x & \mu_{2^1\Sigma-1^1\Pi}(R)\cdot\boldsymbol{E}(t) \\ \mu_{1^1\Sigma-1^1\Pi}(R)\cdot\boldsymbol{E}(t) & \mu_{2^1\Sigma-1^1\Pi}(R)\cdot\boldsymbol{E}(t) & \chi\omega_c\sqrt{2\hbar}\mu_{1^1\Pi}(R)x \end{pmatrix} \tag{5}$$

where $\mathbf{1}$ denotes the unit matrix, μ is the reduced nuclear mass and ω_c is the cavity frequency. $\mu_{ij}(R)$ are the molecular electronic dipole moments between states i and j whereas $\mu_i(R)$ are the diagonal dipole moments at each internuclear distance R, $\boldsymbol{E}(t)$ is the external electric field representing laser pulses and $\Lambda_{1^1\Sigma-2^1\Sigma}(R)$ are the non-adiabatic couplings (NAC) given by

$$\Lambda_{ij}(R) = -\frac{\hbar^2}{2\mu}\left[2\left\langle i\left|\frac{\partial}{\partial R}\right|j\right\rangle(R)\frac{\partial}{\partial R} + \left\langle i\left|\frac{\partial^2}{\partial R^2}\right|j\right\rangle(R)\right], \tag{6}$$

that can be readily computed in this two-state case [3]. The *ab initio* photodynamics of LiF expressed in these equations was implemented in the suite of programs of the

multiconfigurational time dependent Hartree (MCTDH) method [7, 8]. It is important to note that we use undressed states in the molecular basis and the light induced crossing is produced dynamically at the corresponding position R_{LIC} by the cavity interaction, as our simulations in figure 2 show.

C. External laser pulses

Since pulses used in this work are linearly polarized along a given unit vector $\hat{\mathbf{e}}_{\mathrm{p}}$, the total electric field $\boldsymbol{E}(t)$, in the dipole approximation and with a pump-probe delayed scheme, can be written in general form as $\boldsymbol{E}(t) = \boldsymbol{E}_{_{\mathrm{pump}}}(t) + \boldsymbol{E}_{_{\mathrm{probe}}}(t)$, where both laser pulses are described with a harmonic function and a sine squared envelope as follows

$$\boldsymbol{E}_i(t) = \Theta(t - \tau_i + T_i/2)\boldsymbol{E}_{0_i} \sin^2\left[\frac{\pi}{T_i}(t - \tau_i + T_i/2)\right] \sin\left[\omega_i(t - \tau_i + T_i/2)\right] \Theta(T_i/2 + \tau_i - t)\boldsymbol{\epsilon}_{\mathrm{p}}, \tag{7}$$

where T_i is the pulse time duration, ω_i is the central frequency of the pulse, $\Theta(t)$ is the Heaviside function and τ_i is the time delay of the pulses against the initial time set at $t = 0$.

The z-polarized pump pulse initiates the dynamics of the system by transferring part of the population from the ground vibrational state of $1^1\Sigma$ state to the excited electronic $2^1\Sigma$ state. However, in this work a sudden full excitation to the $2^1\Sigma$ state in the Frank-Condon region is assumed, which implies to copy the vibrational ground state to the $2^1\Sigma$ state. The probe pulse, with a time delay with respect to the pump pulse, is prepared with an $(x - y)$-polarization, perpendicular to the pump pulse. Both pulses, separated by time delays of femtoseconds, produce dissociation (through $\Sigma - \Sigma$ transitions because of the pump and $\Sigma - \Pi$ transitions due to the probe) of those LiF molecules oriented along the laboratory z-axis. The probe pulse is used to transfer population from the highly vibrational excited states in the $1^1\Sigma$ electronic state to the dissociative $1^1\Pi$ electronic state. Thus, only the probe pulse is introduced in our dynamical calculations with different chosen delays, without modifying the conclusions of the work. The probe pulse parameters for each cavity frequency used along this work are included in table I.

	$\omega_c = 2.09$ eV	$\omega_c = 2.91$ eV
ω_{probe}	1.5 eV	2.5 eV
T_{probe}	35 fs	35 fs
I_{probe}	7.5×10^{14} W/cm^2	7.5×10^{14} W/cm^2

(8)

TABLE I. Parameters of the probe laser pulse used in this work for LiF, for the two cavity mode frequencies ω_c.

D. Polaritonic propagation using MCTDH

The nuclear TDSE is implemented using MCTDH. The MCTDH package requires the input of the PES in the form of a product of one-dimensional functions. In this particular case, the 2D PES (in R and x coordinates) are given for the three states involved by

$$V_i = E_i(R) + \frac{1}{2}\omega_c^2 x^2 + \chi\omega_c\sqrt{2\hbar}\mu_i(R)x, \tag{9}$$

with $i = (1^1\Sigma, 2^1\Sigma, 1^1\Pi)$, that already meets the MCTDH requirements (i.e., the tool POTFIT included in MCTDH is not required). The nuclear degree of freedom R is defined using a sin-DVR primitive basis with $N_R = 1169$ grid points for internuclear distances between $R = 1.6$ a.u. and $R = 60.0$ a.u. Similarly, the coordinate x corresponding to the cavity mode is described by HO-DVR primitive basis functions with $N_x = 201$ grid points between $x = -25.0$ a.u. and $x = +25.0$ a.u. (large enough to allocate the lowest photon states involved). Thus, the total MCTDH nuclear wave function $\psi(R, x, t)$ reads

$$\varphi(R, x, t) = \sum_{j_R=1}^{n_R}\sum_{j_x=1}^{n_x} A_{j_R j_x}(t)\phi_{j_R}^{(R)}(R, t)\phi_{j_x}^{(x)}(x, t), \tag{10}$$

where $n_R = n_x = 15$ is the number of single particle functions $\phi_{j_q}^{(q)}$ employed for each coordinate q. In order to avoid unphysical reflections, a complex absorbing potential (CAP) is located close to the box edge at $R = 58.5$ a.u., in the grid associated to the vibrational degree of freedom. To obtain dissociation probabilities the dissociating wave packet flux is computed at the position of the CAP.

E. Time-dependent evolution of the polaritonic wave packet

To briefly analyze the non-adiabatic cavity photodynamics we choose the case for $\omega_c = 2.91$ eV. The time evolution of populations and the spatial distributions of the polaritonic probability densities for $1^1\Sigma$, $2^1\Sigma$ and $1^1\Pi$ states are included in figure 2, with a series of snapshots corresponding to those time delays τ at which the dissociation through the $1^1\Pi$ shows a maximum (see figure 3 of main text), i.e., $\tau = 45$, 95 and 141 fs for cavity mode frequency $\omega_c = 2.91$ eV. Let us analyze the main features in these plots. In figure 1, for delay $\tau = 45$ fs and time t_1 the initial $2^1\Sigma$ wave packet (WP) [built as a direct product of the ground vibrational state of LiF times the ground state of the harmonic oscillator (HO) representing the vacuum state $|0\rangle$] is nodeless and it advances in the direction of the LIC. At the passage across the LIC at $R = 6$ a.u. (see time t_2) part of the initial WP transfers to highly excited bound states in the $1^1\Sigma$ state, and one node develops along the x direction due to the transition from the upper HO state $n' = 0$ (vacuum state $|0\rangle$) to the lower HO state $n'' = 1$ (one-photon state $|1\rangle$), thus with the creation of one photon in the cavity. Precisely at this time t_2 the probe laser is active and much of the $1^1\Sigma$ population (the residue remains vibrating) transfers to the $1^1\Pi$ state, which leads to direct dissociation because it is not affected by the NAC. However, at time t_3 we observe the passage of the residual $2^1\Sigma$ WP over the NAC with another exchange of population that results in the $1^1\Sigma$ WP leading to dissociation, but in the Σ channel.

In the case of probe delay $\tau = 95$ fs we appreciate for time t_2 a second passage through the LIC, this time the bound $1^1\Sigma$ WP moves inwards, with some partial reconstruction of the initial $2^1\Sigma$ WP at time t_3. A larger reconstruction of the initial state is seen at time t_3 for delay $\tau = 141$ fs. Moreover, at time t_2 in the latter delay the $1^1\Sigma$ WP moves again outward and crosses the LIC with a resulting portion in the $2^1\Sigma$ state (see time t_3 between the $R_{\rm LIC}$ and the $R_{\rm NAC}$). Another intricate feature at time t_3 in the last delay is that the residual vibrating $1^1\Sigma$ WP interferes with the population transferred through the LIC simultaneously by the reconstructed $2^1\Sigma$ WP and at the same energy, thus producing more complex nodal surfaces. The most important issue at time t_2 is that the $1^1\Pi$ state is populated by the $1^1\Sigma$ WP precisely at the LIC passage, thus producing another maximum in the dissociation yield of the Π channel.

Incidentally we appreciate that for any delay a three-spot feature is always present at

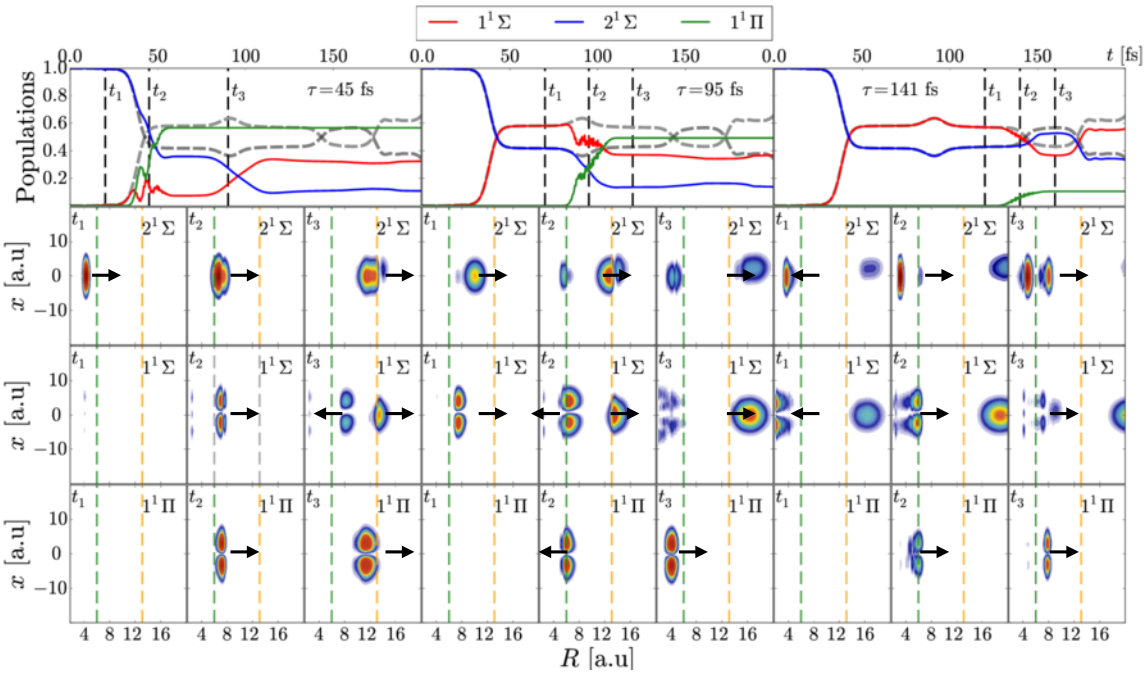

FIG. 2. (First row) Time dependent evolution of $1^1\Sigma, 2^1\Sigma$ and $^1\Pi$ polaritonic populations for a probe laser launched at three different time delays ($\tau = 45, 95, 141$ fs) (solid lines). For comparison the populations in the absence of a probe pulse are also included (dashed lines). The plot corresponds to a cavity mode frequency $\omega_c = 2.91$ eV, probe laser frequency $\omega = 2.5$ eV and interaction factor $\chi = 0.01$. (From second row) Snapshots of the probability density corresponding to the initially excited $2^1\Sigma$ state, the $1^1\Sigma$ ground state and the excited $1^1\Pi$ state (from top to bottom). The polaritonic wave packets move in the PES composed by the molecular PEC of the electronic states, the radiation harmonic oscillator potential plus the diagonal interaction term, according to Eq. (9). Horizontal arrows indicate the direction of the wave packet motion. Snapshots are chosen at three different times t_i for each pump-probe delay τ (before, during and after the arrival of the probe laser). The times t_i represented by black dashed lines in the populations (top) are also indicated in the corresponding plot for the snapshots. Vertical dashed lines within the snapshots indicate the internuclear distance $R_{\rm LIC} = 6.0$ a.u. for the location of LIC and the internuclear distance $R_{\rm NAC} = 13.1$ a.u. for the NAC.

small internuclear distances. It corresponds to low excited vibrational states in the $1^1\Sigma$ state, already populated by the cavity field at a very early stage of the dynamics [3]. In this case the dominant final HO state is $n'' = 2$ (two nodes along x), which corresponds to the creation of two new photons in the cavity, and it is caused by a rapid transition $2^1\Sigma$ to $1^1\Sigma$ (release of one photon) followed by intrastate polariton transitions among the HO states, because of the joint action of the non-negligible diagonal dipole moment $\mu_{1^1\Sigma}(R)$ of LiF. This feature involving states at low vibrational energy is not affected by the external laser pulses, but it is a source of new cavity photons that eventually could be detected along the propagation x-axis of the cavity by using single photon detectors (see figure 1 main text). The creation

of these photons due solely to non-adiabatic effects in the cavity molecular dynamics could be associated to a kind of dynamical Casimir effect.

---

[1] H.-J. Werner *et al*, "Molpro, version 2015.1, a package of ab initio programs," (2015), http://www.molpro.net

[2] A. Tóth, P. Badankó, G. J. Halász, A. Vibók, and A. Csehi, Chemical Physics **515**, 418 (2018), http://www.sciencedirect.com/science/article/pii/S0301010418302817

[3] J. F. Triana, D. Peláez, and J. L. Sanz-Vicario, The Journal of Physical Chemistry A **122**, 2266 (2018), https://doi.org/10.1021/acs.jpca.7b11833

[4] J. Flick, M. Ruggenthaler, H. Appel, and A. Rubio, Proceedings of the National Academy of Sciences **114**, 3026 (2017), http://www.pnas.org/content/114/12/3026.abstract

[5] V. Rokaj, D. M. Welakuh, M. Ruggenthaler, and A. Rubio, Journal of Physics B: Atomic, Molecular and Optical Physics **51**, 034005 (2018), http://stacks.iop.org/0953-4075/51/i=3/a=034005

[6] J. Fregoni, G. Granucci, E. Coccia, M. Persico, and S. Corni, Nature Communications **9**, 4688 (2018), https://www.nature.com/articles/s41467-018-06971-y

[7] G. Worth, M. Beck, A. Jäckle, and H. Meyer, "*The MCTDH Package*, version 8.4," (2007), http://mctdh.uni-hd.de

[8] H. Meyer, F. Gatti, and G. Worth, *Multidimensional Quantum Dynamics: MCTDH Theory and Applications* (John Wiley & Sons, 2009) ISBN 9783527320189